Manuscript aimed at J. Appl. Phys.
This manuscript was accepted by J. Appl. Phys. Click here to see the version of record.

Lattice location study of low-fluence ion-implanted ^{124}In in 3C-SiC

A. R. G. Costa[1*], U. Wahl[2†], J. G. Correia[1], E. David-Bosne[1], V. Augustyns[2], T. A. L. Lima[2], D. J. Silva[3], M. R. da Silva[4], K. Bharuth-Ram[5] and L. M. C. Pereira[2]

1) Centro de Ciências e Tecnologias Nucleares, Instituto Superior Técnico, Universidade de Lisboa, 2695-066 Bobadela LRS, Portugal
2) KU Leuven, Instituut voor Kern- en Stralingsfysica, 3001 Leuven, Belgium
3) IFIMUP and IN-Institute of Nanoscience and Nanotechnology, Departamento de Física e Astronomia da Faculdade de Ciências da Universidade do Porto, 4169-007 Porto, Portugal
4) CICECO, Institute of Materials, Universidade de Aveiro, 13810-193 Aveiro, Portugal
5) Durban University of Technology, Durban 4000, South Africa

Abstract

We report on the lattice location of low-fluence ion implanted ^{124}In in single-crystalline 3C-SiC by means of the emission channeling technique using radioactive isotopes produced at the ISOLDE/CERN facility. In the sample implanted at room temperature to a fluence of 4×10^{12} cm^{-2}, 60(9)% of the In atoms were found slightly displaced (0.12-0.20 Å) from substitutional Si sites, with the remainder occupying sites of low crystallographic symmetry, the so-called 'random' sites. For 800 °C implantation, the substitutional In fraction increased to 72(8)% and the displacements from ideal substitutional Si sites were reduced to those expected for the lattice vibrations. These results, in terms of lattice location and disorder, are compared to those on In implanted group IV semiconductors silicon and diamond.

Keywords: emission channeling, lattice location, ion implantation, 3C silicon carbide, *p*-type electrical dopant, implantation damage

I. Introduction

Silicon carbide is a wide band gap semiconductor which, due to its electrical and thermal stability, is suitable for high power, high voltage, high frequency and high temperature applications [1-3]. Among the advantages of SiC in comparison to most other wide gap semiconductors, are the facts that both *n*- and *p*-type doping are possible, that ion implantation is successful in the introduction of dopants, and that SiC possesses SiO_2 as passivating native oxide. All of these characteristics are shared with conventional Si technology. While doping

* Author to whom correspondence should be addressed: angelo.rafael.granadeiro.costa@cern.ch
† On leave from Centro de Ciências e Tecnologias Nucleares, Instituto Superior Técnico, Universidade de Lisboa

during growth allows producing homogeneously doped SiC bulk substrates or epitaxial layers, ion implantation is widely used to create thin doped layers in SiC devices [4]. A particular drawback of ion implantation into SiC is that it requires high-temperature annealing in order to remove implantation defects and electrically activate the dopants. While process simulators are being developped in order to predict the electrical activation of implanted dopants as a function of chosen annealing procedure in SiC, such tools are still based on a phenomenological approach without detailed understanding of the underlying microscopic processes [5]. On the other hand, in Si technology, which is much more advanced, detailed models of the kinetics of radiation damage on a microscopic level are beginning to play a role in process simulation for industrial applications [6].

For the *n*- or *p*-type doping of SiC, elements of the VA or IIIA group of the periodic table are used, respectively. Due to the deep-level related issues with boron mentioned below, aluminium is the most commonly used *p*-type dopant, while for *n*-type doping nitrogen or, less frequently, phosphorus is used as dopant. It is generally assumed that the size of the dopants in comparison to Si and C defines their preferred positions inside the SiC lattice; thus Al and P should substitute for Si lattice atoms while N should replace C [7-9]. This site preference is underlying the approach, as described in detail by Larkin *et al*. [7], of choosing Si- or C-rich growth conditions in order to facilitate or hinder incorporation of site-specific dopants during SiC epitaxial growth. Direct experimental data, however, on the lattice location of dopants in SiC are quite scarce, although they are crucial in order to understand their properties as dopants. This is illustrated by the case of the lattice sites of boron, which, initially, from electron paramagnetic resonance (EPR) studies, was reported to occupy the C-site [10]. However, later studies also based on EPR results, concluded that the B dopants were incorporated mainly in substitutional Si sites [11]. Theoretical considerations [9, 12], on the other hand, suggest that both sites are possible but result in shallow (B_{Si}) or deep acceptors (B_C), respectively, although for the deep B acceptor more complicated models have also been proposed.

One of the issues that complicates the practical use of SiC is the relatively large dopant ionization energies, in particular for the acceptors. Therefore alternative dopants or doping procedures that introduce shallow levels with low ionization energies are highly desirable [9] and have been actively explored. Ga doping of 4H-SiC by means of ion implantation has recently been addressed using electrical characterization methods as well as density functional theory [13]. For that element, previous Rutherford Backscattering Spectroscopy/Channeling (RBS/C) experiments had shown its substitutional incorporation on Si sites in 6H-SiC,

following room temperature ion implantation at the very high fluence of 5×10^{15} cm^{-2} and annealing at 1200 °C [14]. There exists very little experimental information with regards to indium doping of SiC. From the theoretical point of view, Miyata *et al*. [15] investigated the ionization energies of several substitutional group II, III, V and VI impurity atoms in 4H-SiC. For In the calculations suggest that this element should be an acceptor, with ionization levels as deep as the Al ones. While In was discussed briefly in the review made by Lebedev [8], the author stated that it was not possible to obtain *p*-type SiC from doping with In during crystal growth. An early attempt [16] on ion implantation doping of 3C- and 6H-SiC found no *p*-type conduction when In was implanted at room temperature but weak *p*-type behaviour could be achieved in 6H-SiC when the implantation was performed at 350 °C. These authors, from RBS/C studies, also reported high fractions of substitutional In following annealing at 1200 °C, although no distinction could be made between In on Si or C sites.

In the present contribution we present a lattice location study of the low-fluence implanted radioactive isotope ^{124}In in 3C-SiC by means of the emission channeling technique. The preference of In for substitutional Si sites is unambiguously established and no other highly-symmetric lattice sites appear to be occupied. Our results show that most In atoms are already incorporated close to substitutional Si sites during room temperature implantation, although their root mean square displacement from the ideal Si sites indicates the presence of nearby defects. Increasing the implantation temperature to 600 °C and above results in In incorporation on ideal substitutional Si sites. The lattice location and defect situation found in this work for SiC are compared to In implanted in the group IV semiconductors silicon and diamond.

II. Experiment

The lattice location of the radioactive isotope ^{124}In implanted into a 3C-SiC single crystal was investigated by means of the emission channeling (EC) method [17, 18]. This technique is based on the observation of the anisotropic intensity patterns of emitted β^- particles when the radioactive probe atoms are embedded in single crystals. For that purpose, the ^{124}In beams at CERN's on-line isotope separator facility ISOLDE were used, which provides mass-separated and chemically clean beams of radioactive isotopes [19-20]. ^{124}In was produced by fission of a uranium carbide UC_2 target induced by 1.4 GeV proton beams from the CERN PSB, followed by chemically selective laser ionization and electromagnetic mass separation. The mass 124 beams actually consisted of a mixture of 73% ^{124}In ($t_{1/2}$=3.17 s) in its ground state and 27% of isomeric ^{124m}In ($t_{1/2}$=2.4 s), with both ^{124}In states decaying to the stable isotope ^{124}Sn by means

of β^- emission. Since both ^{124}In and ^{124m}In are short-lived isotopes with half-lives of a few seconds only, all EC measurements were performed on-line with implantation and measurement taking place simultaneously, first at room temperature (RT) and subsequently at elevated temperatures, in vacuum better than 10^{-5} mbar. Measurements at temperatures up to 800 °C were made possible by the use of an aluminated mylar foil in front of the Si position-sensitive electron detector, which shielded it from the light emitted by the glowing sample.

An undoped single-crystalline 3C-SiC sample (Hoya Corporation, Japan) with <100> oriented surface was used. The implantation current of 50 keV ^{124}In was 0.6 pA in a beam spot of 1 mm diameter, corresponding to a fluence rate of 4.8×10^{8} cm^{-2}/s; the total implanted fluence at the end of the experiment was ~1×10^{13} cm^{-2}. SRIM [21] simulations yield a Gaussian implantation profile with projected range, straggle and peak concentration of 232 Å, 61 Å and 6×10^{18} cm^{-3}, respectively, and that each implanted In ion produces approximately 800 vacancies and interstitials.

An overview of the major lattice sites in the cubic 3C-SiC structure is shown in Fig. 1. In order to quantitatively analyze the experimental data, theoretical β^- emission patterns were calculated for a large variety of sites within the 3C unit cell, including all of the substitutional and interstitial sites specifically indicated in Fig. 1, but also for displacements along <111>, <100> and <110> axial directions in between the major lattice sites. Simulations were also performed for emitter atoms which are isotropically displaced around substitutional Si and C sites with Gaussian probability distributions of root mean square (rms) values from 0.04-0.5 Å. The calculation of theoretical emission patterns used the "*many-beam*" approach [17-18]. The fact that the probe beam consisted of a mixture of ^{124}In nuclei in two states with different β^- energy spectra [endpoint energies $E_{\beta,max}$(^{124}In)=6227 keV and $E_{\beta,max}$(^{124m}In)=4843 keV, average β^- energies $\langle E_\beta \rangle$(^{124}In)=2045 keV and $\langle E_\beta \rangle$(^{124m}In)=1609 keV] was taken into account when performing the *many-beam* simulations. The resulting normalized theoretical emission patterns, $\chi_{theo}(\vartheta,\varphi)$, where ϑ and φ denote polar and azimuthal angles from the axis, were smoothed using a Gaussian width of $\sigma = 0.1°$ to account for the contribution to the angular resolution from the 1 mm diameter beam spot on the sample. Details on the experimental conditions, the *many-beam* simulations, the approach to the fitting process and the correction procedure for background of scattered β^- and γ particles are provided in our previous publication on lattice location of transition metals in 3C-SiC [22].

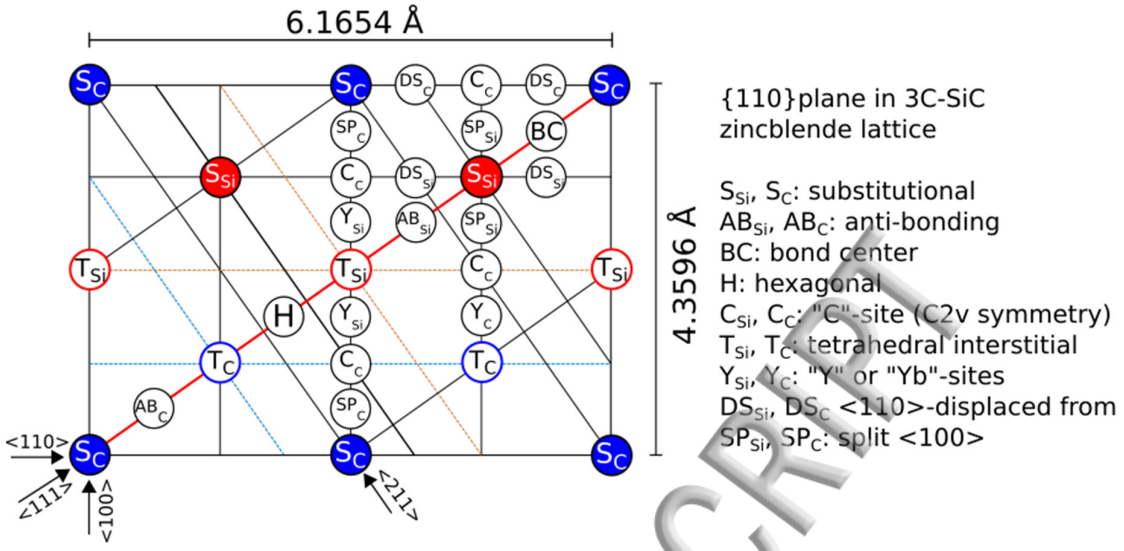

FIG 1. Cross-section through the 3C-SiC zincblende unit cell along a {110} plane showing the Si and C lattice positions and the main interstitial sites. Note that along the <111> direction the substitutional (S_{Si} and S_C) and tetrahedral interstitial (T_{Si} and T_C) sites are all located on the same row; along the <100> direction S_{Si} is on the same row as T_C while S_C is on the same row as T_{Si}.

III. Results and discussion

The two-dimensional patterns in Fig 2(a)-(b) show the angular dependence of the measured β^- emission yields in the vicinity of the <110> and <211> directions of the 3C-SiC sample during 600 °C implantation of ^{124}In. Note that for these two crystallographic directions each of the positions inside the crystal lattice shown in Fig. 1 results in a characteristic emission pattern with distinct anisotropies and thus allows for the unambiguous identification of the occupied lattice sites. The fact that prominent channeling is observed along the <110> and <211> axes and the closest-packed planes {110}, {111} and {100} is clear evidence that the majority of In probes are located on substitutional sites. Visually comparing the experimental <110> and <211> patterns with the corresponding simulated patterns for 100% of ^{124}In on ideal S_{Si} sites [Fig. 2(c)-(d)] and 100% on ideal S_C sites [Fig. 2(e)-(f)] indicates that S_{Si} sites provide a better match, in particular for the relative intensity of planar channeling effects. A quantitative analysis, which unambiguously identifies the major lattice site as well as providing insight into possible minority sites, is achieved by fitting the experimental patterns with linear combinations of theoretical patterns, as is outlined below.

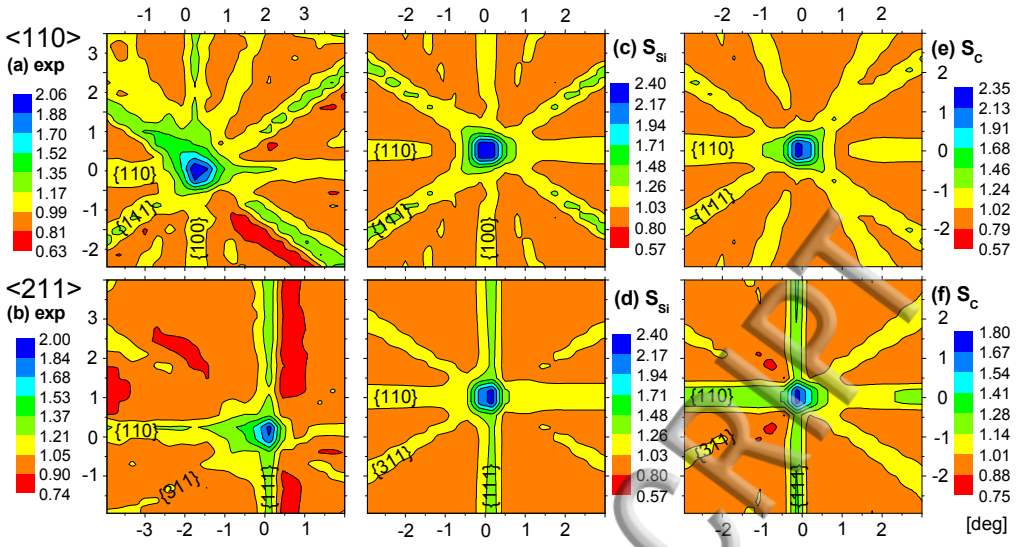

FIG 2. (a)-(b) Experimental ^{124}In β^- emission patterns around the <110> and <211> axes of 3C-SiC during 600 °C implantation. The theoretical patterns for 100% of ^{124}In on the ideal substitutional Si sites (S_{Si}) (c)-(d) and ideal substitutional C sites (S_C) (e)-(f) sites are shown for comparison.

Figure 3(a)-(d) and (i)-(l) show the β^- emission yields measured around all four directions <100>, <110>, <111> and <211> during RT and 600 °C implantations, respectively. While the maximum anisotropy of the electron emission yields increased by 35-60% between RT and 600 °C implantation, no other major changes are directly obvious in the patterns. In order to identify and quantify the major lattice sites, initially only single fractions on ideal lattice sites were considered when fitting the experimental patterns. This confirmed that indeed the majority of emitters are located close to the substitutional Si site (S_{Si}) at both implantation temperatures. In a next step we investigated possible displacements of the ^{124}In probe atoms from the ideal S_{Si} site by allowing for displacements along <111>, <100> or <110> directions towards interstitial sites. In case of RT implantation such displacements up to 0.2 Å clearly improved the chi square of fit but the improvements were of similar value irrespective of the chosen direction of displacement. Correspondingly the same improvements in quality of fit could be achieved if, instead of displacements along specific crystallographic directions, isotropic Gaussian probability distributions centered at S_{Si} sites but with specific rms amplitudes u_1 were considered. The best fit rms displacements u_1 from ideal S_{Si} sites were scattered around 0.12-0.20 Å for RT implantation but were considerably smaller (0.07-0.11 Å) following 600 °C implantation, cf Fig. 4. The corresponding best fits to the experimental patterns have been included in Fig. 3, yielding 60(9)% on S_{Si} for RT [Fig. 3(e)-(h)] and 69(4)% for 600 °C implantation [Fig. 3(m)-(p)].

Next, the possibility for more than one regular site being occupied was explored by fitting the experimental data with a linear combination of the theoretical patterns from S_{Si} plus a second site. Although In probes on substitutional carbon sites S_C as well as tetrahedral interstitial Si-coordinated (T_{Si}) or tetrahedral interstitial C-coordinated (T_C) sites were of special interest, the fitting procedure was also carried out for all of the other sites for which the channeling patterns were simulated. However, the improvements in fit quality were not significant and/or the fractions resulting from fits of different directions were not consistent. For example, while the combination of (S_{Si}+S_C) sites improved the χ^2 of fit by a few per cent, the small resulting fractions on S_C sites were positive for the fits of the <211> patterns but negative in case of the <110>, leading to the conclusion that the possible fractions of In on regular sites other than S_{Si} are at maximum in the few per cent range. This is in contrast to the case of the implanted transition metals Mn, Fe and Ni, where we have found large fractions on tetrahedral interstitial T_C sites in addition to substitutional Si sites, both in 3C-SiC [22] and in 6H-SiC [23]. Note that substitutional S_{Si} fractions for ^{124}In are below 100%, i.e. a significant amount of probes is situated on so-called 'random' sites, which contribute with an isotropic emission yield. These 'random' sites correspond to positions of low crystallographic symmetry or with very disordered or amorphous surroundings.

The fraction of In at substitutional Si sites (S_{Si}) and the rms displacements as a function of implantation temperature are shown in Fig. 4. As can be seen, with increasing implantation temperature the substitutional fraction of In grows moderately from 60% at RT to 72% at 800 °C, while at the same time the rms displacements become significantly smaller. As a reference, the thermal vibration amplitude u_1(Si) of Si in SiC as function of temperature is shown by the dashed lines in Fig. 4(a). In the RT implanted state the rms displacement of ^{124}In is larger than the vibration amplitude u_1(Si), showing that In atoms are not perfectly incorporated in S_{Si} sites. Implanting at 600 °C the In displacements decrease to approximately the value of u_1(Si) at that temperature, which indicates the incorporation of In into the perfect substitutional Si site, although with fractions still below 100%.

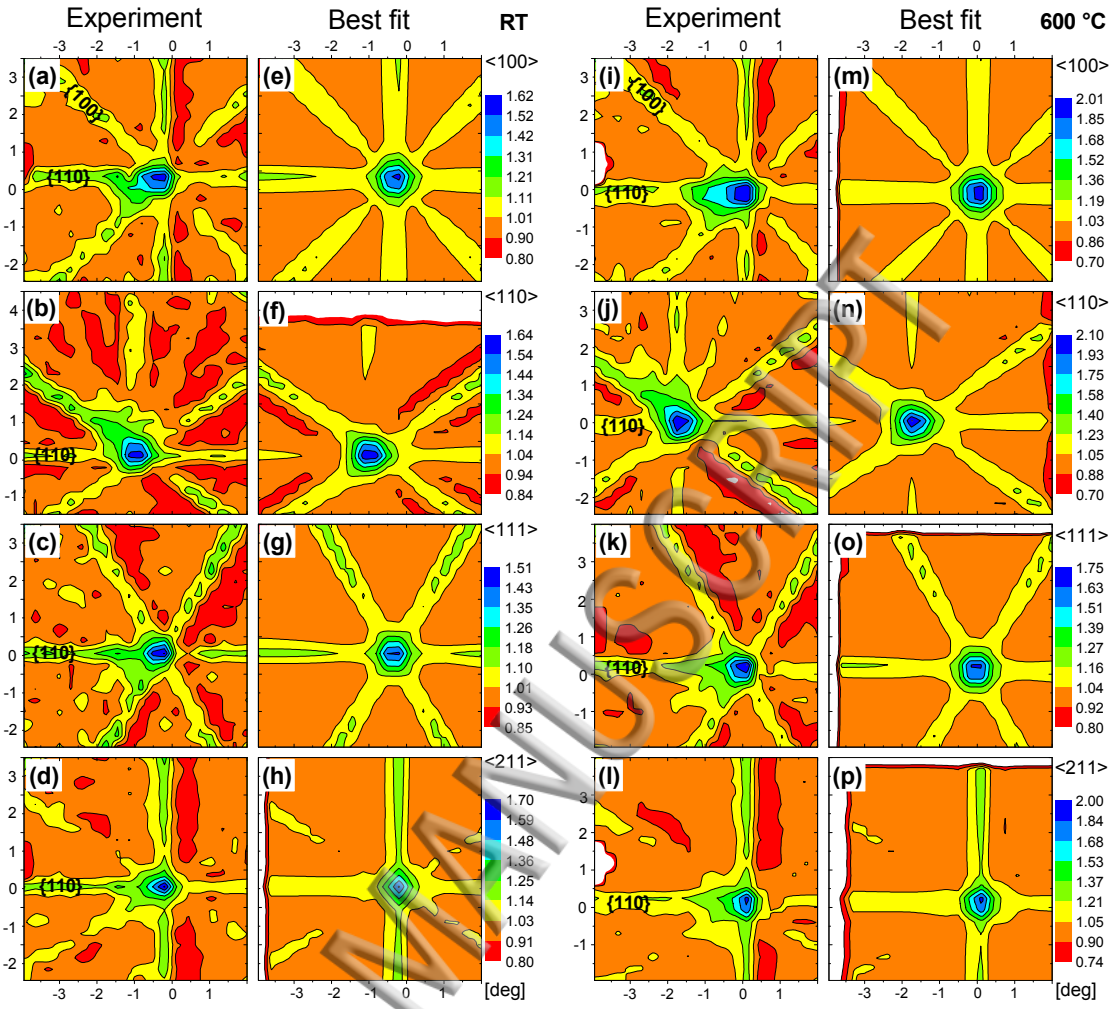

FIG 3. Experimental ^{124}In β^- emission channeling patterns in the vicinity of <100>, <110>, <111> and <211> directions during RT (a)-(d) and 600 °C (i)-(l) implantation into 3C-SiC. The plots (e)-(h) and (m)-(p) are the corresponding best fits of theoretical patterns considering only substitutional In sites but with rms displacements u_1 according to Fig. 4(a), Note that in some cases the crystal was oriented during the experiment in such a way that the recorded patterns included areas which were further than 3° away from a major crystallographic direction. Since the *many-beam* simulations were restricted to an angular range of ±3° from the axes, the corresponding areas in the best-fit patterns (f), (m), (o) and (p) beyond this range are shown in white.

In the following we discuss our findings in relation to previous results on In implantations from the literature, taking into account also general features of ion implantation and defect annealing in SiC. Ion implantation results in the creation of defects, the accumulation of which can ultimately induce amorphization. However, detrimental dopant-defect interactions already exist at low levels of damage and are usually considered as the reason why the implanted dopants are not electrically active after the implantation process: the electrical activation of ion implanted dopants requires both their incorporation on the proper lattice sites, i.e. usually substitutional sites, plus the removal of electrically compensating defects resulting from the

implantation damage. While SiC presents high radiation hardness due to its high bond-strength, this also means that lattice damage produced by the ion implantation process needs very high annealing temperatures, usually above 1500 °C, in order to recover and to activate the implanted dopants [1, 2, 4, 5, 24]. While in Si, Ge or GaAs technology it is common to purposely amorphize the implanted region and epitaxially regrow it during annealing, this approach is not feasible in SiC due to the considerable difficulty of removing all defects. Instead, the approach is to minimize the impact of damage already during implantation by keeping implanted fluences as low as possible, using low mass implants or raising the implantation temperature [4]. The damage density above which a crystalline structure turns amorphous, is often expressed by the number of displacements needed per host atom (dpa). For SiC at RT this threshold is crossed if implanted ions have created ~0.45 dpa [25] which corresponds to ~4×10^{22} vacancies/cm^3 (the SiC atomic density is 9.65×10^{22} atoms/cm^3). SRIM simulations [21] indicate that initially around 400 Si vacancies, as well as a similar number of C vacancies and corresponding interstitials are created per implanted 50 keV In atom. The In fluence accumulated during the RT analysis of our sample was only 4×10^{12} cm^{-2} corresponding to an In peak concentration of 2.4×10^{18} cm^{-3} from which one estimates 0.02 dpa, well below the RT amorphization threshold.

On the basis of *ab initio* calculations, Miyata *et al*. predicted that In impurities prefer to substitute on silicon rather than carbon sites in 4H-SiC [15], which is clearly confirmed by our emission channeling experiments, though for 3C-SiC. The only previous study that could be found in the literature reporting on direct lattice location of In in SiC is the work of Hart *et al* [16], which was already briefly mentioned in the introduction. Following implantation of 40 keV In ions at fluences above 10^{14} cm^{-2} into 3C- and 6H-SiC at different temperatures, RBS/C was used to assess the damage situation and possible lattice sites of In. For RT implantation at these fluences, the implanted layer was found to be completely amorphous, while our studies at about a factor 25 lower fluence revealed a still largely intact SiC lattice with already ~60% substitutional In for RT implantation. Ref. [16] also showed that following implantation of 3×10^{14} cm^{-2} at 450 °C and annealing at 1200 °C, ~90% of In atoms were aligned with <100> and <110> directions in 3C-SiC, and ~95% with the c-axis in 6H-SiC after 350 °C implantation of 1×10^{14} cm^{-2} and 1200 °C annealing. However, since the backscattering yield from In was only measured in random directions and fully aligned with the <100> and <110> in 3C and [0001] in 6H, it could not be distinguished whether the In atoms are aligned with rows of Si or C atoms, hence whether they prefer substitutional Si or C sites. Sublattice location would have

required the measurement of full angular scans, as was performed by [14] for the case of Ga. In contrast, since the emission channeling method measures complete two-dimensional angular patterns around the major crystallographic directions, we were able to unambiguously establish the preference of In for substitutional Si sites. The maximum substitutional fraction that we achieved following implantation at 800 °C, though, was 72%, well below the 90-95% mentioned in Ref. [16] after 1200 °C annealing, showing that some implantation damage remained in our sample.

References [26-28] studied the formation and stability of defect complexes formed by RT implantation of the radioactive isotope ^{111}In in 3C-, 4H- and 6H-SiC using Perturbed Angular Correlation (PAC) spectroscopy. Although the implanted fluences are not specifically given, the fact that in Ref. [26] ^{111}In peak concentrations of 10^{18} cm^{-3} are mentioned for 350 keV implantation, allows one to estimate that the fluences should have been around 1.3×10^{14} cm^{-2}, thus in the RT as-implanted state the implanted region should have been amorphized. Correspondingly, no ^{111}In was found in cubic surroundings in the as-implanted state in 3C-SiC, but a fraction of 30% was achieved once the sample was annealed at 1300 °C. While the In in cubic surroundings was assigned to substitutional Si sites, definite proof could not be given since also substitutional C and both tetrahedral interstitial sites are characterized by cubic surroundings in 3C-SiC. For ^{111}In probe atoms in 4H- and 6H-SiC up to five different defect configurations were identified, however, only 1-2 of them were assigned to resulting from simple lattice electrical field gradients on substitutional Si sites. Following annealing at T_A=700 °C, 9% of ^{111}In probe atoms in 4H-SiC were found in the assumed S_{Si} configuration, which increased to 17% following annealing at T_A=1500 °C; in 6H-SiC the corresponding values were 2% for T_A=700 °C and ~19% for T_A=1100 °C. Thus, the possible substitutional In fractions are considerably lower than in our low-fluence study but also lower than in Ref. [16] that used hot implantation. Above T_A~1000 °C the authors also reported the appearance of PAC signals that were assigned to In-V_C complexes with C vacancies, however, this temperature range was not within reach of our on-line emission channeling experiment.

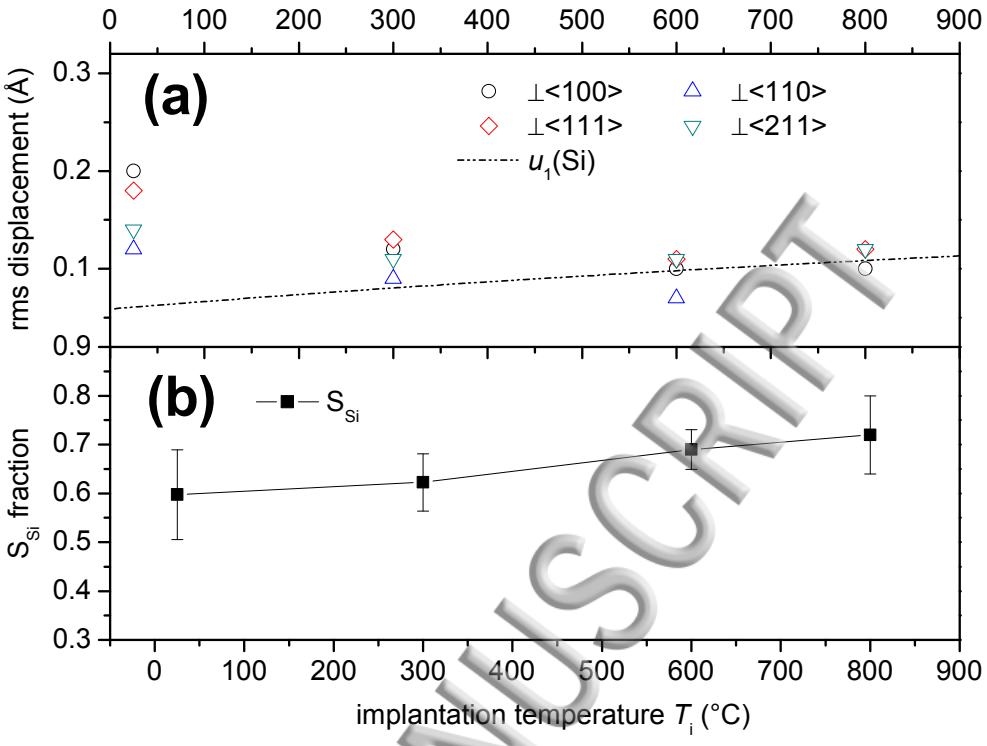

FIG 4. (a) One-dimensionally projected isotropic rms displacements perpendicular to the channeling axes, from the fits as a function of implantation temperature. The dashed line corresponds to the thermal vibration amplitude u_1(Si) of Si in SiC, calculated for a Debye temperature T_D(Si)=692 K [22]. Note that, assuming the Debye temperature of In on Si sites scales with $T_D(^{124}\text{In}) = T_D(^{28}\text{Si})[28/124]^{1/2}$=329 K, would lead to values for $u_1(^{124}\text{In})$ that are only minimally lower than $u_1(^{28}\text{Si})$, e.g. 0.0506 Å *vs* 0.0548 Å at RT and even less at higher temperatures. The corresponding curve is not shown since it would be indistinguishable from the one for Si. Panel (b): Fitted fractions of ^{124}In emitter atoms on substitutional Si sites as a function of the implantation temperature, averaged from the four measured crystallographic directions with the error bars representing the spread in fitted fractions.

Although a considerable part of the implantation-induced damage in SiC can be removed at 1200 °C, to achieve reasonable electrical activation annealing at temperatures in excess of 1500 °C is required, as was already mentioned. Even in this case post-implant annealing alone may not be sufficient, and performing high-temperature implantations is a viable method in use today by the industry as it can mitigate the damage formation. The detrimental action of radiation damage on the electrical activity of nitrogen donors in SiC has been investigated by Åberg *et al* [29]. They found that in *n*-type SiC free electron concentrations are severely depleted following the irradiation with MeV ions of H, He, B and Al, but that the effect can be considerably reduced at irradiation temperatures above 600 °C. For the doping of SiC by means of ion implantation of N, P, Al or B, implantation temperatures around 400-600 °C followed by post-implant annealing at 1500-1700 °C are usually chosen [4, 24]. Our study shows that in the case of In a

particular effect of hot implantation is to reduce the defects in the immediate neighbourhood of In and thus directly improve its incorporation on ideal Si sites.

To date, no report about the experimental measurement of the In acceptor ionization energy has been made. In the *ab initio* calculation study by Miyata *et al.* [15] the acceptor ionization energy of In in 4H-SiC was predicted as $E_a(Si_h)$~150 meV and $E_a(Si_k)$~260 meV. As a comparison, the Al ionization energy in 3C-SiC, at the substitutional Si site, is $E_a(Si)$=254 meV [30], and in 4H-SiC is $E_a(Si_h)$=197.9 meV and $E_a(Si_k)$=201.3 meV [31]. The values calculated by Miyata *et al.* are similar to the ones experimentally obtained for Al, which implies that In can be an option as a shallow acceptor to Al if one considers only the ionization energy values. However, the reported In solubility (9.5×10^{16} cm^{-3} at 2500 °C) is 4-5 orders of magnitude lower than the solubility of Al (2×10^{21} cm^{-3}) [32], which should undoubtedly limit the applicability of In as an electrical dopant. On the other hand, since Hart [16] has already reported successful substitutional In incorporation of $>10^{20}$ cm^{-3} by means of ion implantation, solubility might actually not be a limiting factor either.

Finally, it will be interesting to compare the current experiment on ^{124}In in 3C-SiC to previous lattice location results for the same element in the group IV semiconductors diamond and silicon. Concerning In implanted Si, Lindner *et al.* [33] reported 55-60% of ^{112m}In and ^{114m}In probes located at substitutional Si sites directly after RT implantation at fluences of 10^{11} cm^{-2}. Upon annealing at 427 °C an increase of ~30% in the channeling yield was observed and attributed to the rearrangements of In atoms and removal of radiation damage inside the Si lattice. Alves *et al.* [34] complemented the previous low-fluence emission channeling work with RBS/C lattice location studies of In implanted into Si at high fluence. Following RT implantation of 10^{15} cm^{-2} In, the implanted region was found to be amorphous, but upon annealing and epitaxial regrowth at 550 °C they reported an In fraction of 50% located at substitutional Si sites. Subsequent annealing at higher temperatures resulted in decrease of substitutional In, which was attributed to the formation of In precipitates. Concerning In in diamond, both Hofsäss *et al.* [35] and Quintel *et al.* [36] reported strong conversion electron emission channeling effects corresponding to ^{111}In probes located at substitutional C sites after annealing in the temperature range 1000 °C-1200 °C with fractions reaching a maximum of 45%. ^{111}In probes located at interstitial sites were also considered by both authors, but estimated below 10%. Bharuth-Ram *et al.* [37] reached similar results, reporting an ^{111}In fraction of 32% on substitutional C sites, however, in this case after annealing at 1200 °C they also identified a fraction of 10% of In on tetrahedral interstitial sites. The emission channeling lattice location

experiments of In in Si [33] as well as the ones on In in diamond from Refs. [35-37] did not use position-sensitive detection of emitted electrons, measuring only one-dimensional angular scans of the electron yield which provide less information. The only study that used complete two-dimensional patterns for lattice location of ^{111}In in diamond is the one of Doyle *et al* [38]. Following RT implantation and annealing at 1100 °C they identified 22-31% on ideal substitutional sites, however, the major fraction of 45-59% was assigned to a position that is displaced by ~0.45 Å from the S to the bond-center sites, which was interpreted as In inside a complex involving a double vacancy. The exact lattice location distribution of implanted In in diamond thus remains controversial. In our measurements on 3C-SiC we checked for the occupancy of all of these non-substitutional sites, the outcome, however, was negative.

SiC, Si and diamond will all suffer amorphization if the damage produced by the ion implantation process surpasses the damage density threshold. As was already mentioned, for SiC at RT this threshold is crossed if implanted ions have created ~4×10^{22} vacancies/cm^3 (~0.45 dpa at an atomic density of 9.65×10^{22} atoms/cm^3) [25]; for diamond the critical damage level is found to be only ~10^{22} vacancies/cm^3 (~0.06 dpa at 1.76×10^{23} atoms/cm^3) [39]; for Si values from ~10^{21}-10^{22} vacancies/cm^3 (0.02-0.2 dpa at 4.99×10^{22} atoms/cm^3) can be found in the literature [40]. An approximate estimate of the maximum concentrations of vacancies/cm^3 from the implantation energies and the In implantation fluence range used in the EC studies on diamond [35-38] and Si [33] yields ~10^{21} vacancies/cm^3 and 3×10^{19} vacancies/cm^3, respectively, in comparison to 10^{21} vacancies/cm^3 for our present SiC experiment. In all cases, the very low fluences that can be probed using emission channeling have allowed performing lattice location experiments directly in the as-implanted state, which requires staying below the threshold for amorphization. As is outlined in Refs. [6, 40], understanding in greater detail the nature of isolated collision cascades formed upon ion implantation, is highly desirable in order to assess the validity of atomistic theoretical modelling. In that respect, due to the reduced size of isolated collision cascades, experimental methods are required that can identify such cascades and the related damage levels. For instance, the formation of so-called “amorphous pockets” has often been proposed upon the implantation of heavy ions such as In [6, 40]. Emission channeling can here provide additional insight since each implanted radioactive probe is located directly inside the collision cascade which it created during its implantation. The fact that emission channeling effects due to substitutional In could already be measured in the RT as-implanted state in Si, SiC and diamond, therefore proves that in the case of isolated

collision cascades a significant fraction of In probe atoms are not located in totally amorphous pockets.

IV. Conclusions

As described in this work, the lattice location of In ions implanted in 3C-SiC was experimentally determined. Our results confirm theoretical predictions suggesting that In atoms are most stable on substitutional Si sites [15]. While we checked for the occupation of positions other than substitutional Si, no such sites could be identified. The fits of the experimental patterns after RT ion implantation assign 60(9)% of the implanted In dopants to S_{Si} sites with rms displacements of 0.16-0.20 Å, a value that is higher than expected from thermal vibrations only. Since a considerable amount of vacancies and interstitials are created during the implantation process, the extra displacement is most likely caused by the presence of defects that remain in the vicinity of the In atoms. Implantation at 600 °C promotes substitutional In with rms values similar to the thermal vibration amplitude u_1(Si) of the Si atoms in the host lattice, confirming the substitutional incorporation of In at ideal Si sites. For 800 °C implantation, an increase in the substitutional In fraction to 72(8)% was observed. The increase in the In substitutional fraction and in particular the promotion of the location of In to ideal S_{Si} sites in the temperature range 300 °C-600 °C are a clear indication of the recovery of the host lattice. For the RT implantations the accumulated fluence stayed below 4×10^{12} cm^{-2}, a regime that is still characterized by isolated collision cascades. Our results, hence, show, that if amorphous pockets do exist in the vicinity of the implanted In ions, only a fraction of at most ~40% of the In ions should be located inside them.

Acknowledgements

We acknowledge the beam time provided by the ISOLDE collaboration. This work was funded by the Portuguese Foundation for Science and Technology (FCT) through project CERN-FIS-PAR-0005-2017 and the strategic project UID/Multi/04349/2013, by the FWO Vlaanderen and the KU Leuven (STRT/14/002). ARG Costa is thankful for the FCT grant SFRH/BD/86386/2012. KBR acknowledges support from the South African Department of Science and Technology through the SA-CERN Program. The ISOLDE beam times were supported by the European Commission through the Horizon 2020 program (grant number 654002 ENSAR2).

References

[1] M. Willander, M. Friesel, Q. U. Wahab, and B. Straumal, "Silicon carbide and diamond for high temperature device applications", J. Materials Science: Materials in Electronics **17**, 1–25 (2006).

[2] T. Kimoto, "Material science and device physics in SiC technology for high-voltage power devices", Jpn. J. Appl. Phys. **54**, 1–27 (2015).

[3] G. Liu, B. R. Tuttle, and S. Dhar, "Silicon carbide: A unique platform for metal-oxide-semiconductor physics", Appl. Phys. Rev. **2**, 021307 (2015).

[4] A. Hallén and M. Linnarsson, "Ion implantation technology for silicon carbide", Surface & Coatings Technol. **306**, 190–193 (2016).

[5] V. Simonka, A. Toifl, A. Hössinger, S. Selberherr, and J. Weinbub, "Transient model for electrical activation of aluminium and phosphorus-implanted SiC", J. Appl. Phys. **123**, 235701 (2018).

[6] L. Pelaz, L. A. Marqués, M. Aboy, P. López, and I. Santos, "Improved physical models for advanced silicon device processing", Materials Science in Semiconductor Processing 62, 62-79 (2017).

[7] D. J. Larkin, "SiC dopant incorporation control using site-competition CVD", Phys. Stat. Sol. (b) **202**, 305-320 (1997).

[8] A. Lebedev, "Deep level centers in silicon carbide: A review", Semiconductors **33**, 107-130 (1999).

[9] P. Deák, B. Aradi, A. Gali, and U. Gerstmann, "Some like it shallower – *p*-type doping in SiC", Phys. Stat. Sol. (b) **235**, 139-145 (2003).

[10] H. H. Woodbury and G. W. Ludwig, "Electron spin resonance studies in SiC", Phys. Rev. **124**, 1083-1089 (1961).

[11] A. G. Zubatov, I. M. Zaritskii, S. N. Lukin, E. N. Mokhov, and V. G. Stepanov, "Electron

spin resonance in boron-doped silicon carbide", Sov. Phys. Solid State **27**, 197-201 (1985).

[12] M. Bockstedte and O. Pankratov, "*Ab initio* study of intrinsic point defects and dopant-defect complexes in SiC: application to boron diffusion", Mater. Sci. Forum **338-342**, 949-952 (2000).

[13] G. Alfieri, L. Knoll, L. Kranz, R. Minamisawa, and V. Sundaramoorthy, "Point defects in Ga-implanted SiC: Experiments and theory", J. Appl. Phys. **121**, 245703 (2017).

[14] M. Satoh, Y. Nakaike, and K. Kuriyama, "Preferential ion scattering from 6H-SiC: Identification of the substitutional site of the implanted Ga impurities", J. Appl. Phys. **89**, 61–65 (2001).

[15] M. Miyata, Y. Higashiguchi, and Y. Hayafuji, "*Ab initio* study of substitutional impurity atoms in 4H-SiC", J. Appl. Phys. **104**, 123702 (2008).

[16] R. R. Hart, H.L. Dunlap, and O.J.Marsh, "Backscattering analysis and electrical behavior of SiC implanted with 40 keV indium", Ion Implantation in Semiconductors ed I. Ruge and J. Graul (Springer, Berlin, Heidelberg, 1971) pp. 134–140.

[17] H. Hofsäss and G. Lindner, "Emission channeling and blocking", Physics Reports **201**, 121-183 (1991).

[18] U. Wahl, "Advances in electron emission channeling measurements in semiconductors", Hyperfine Interact. **129**, 349-370 (2000).

[19] R. Catherall, W. Andreazza, M. Breitenfeldt, A. Dorsival, G. J. Focker, T. P. Gharsa, T. J. Giles, J. L.Grenard, F. Locci, P. Martins, S. Marzari, J. Schipper, A. Shornikov, and T. Stora, "The ISOLDE facility", J. Phys. G: Nucl. Part. Phys. **44**, 094002 (2017).

[20] K. Johnston, J. Schell, J.G. Correia, M. Deicher, H.P. Gunnlaugsson, A.S. Fenta, E. David-Bosne, A.R.G. Costa, and D.C. Lupascu, "The solid state physics programme at ISOLDE: recent developments and perspectives", J. Phys. G: Nucl. Part. Phys. **44**,

104001 (2017).

[21] J. F. Ziegler, M. D. Ziegler, and J. P. Biersack, "SRIM- The stopping and range of ions in matter (2010)", Nucl. Instruments Methods Phys. Res. B **268**, 1818-1823 (2010).

[22] A. R. G. Costa, U. Wahl, J. G. Correia, E. Bosne, L. M. Amorim, V. Augustyns, D. J. Silva, M. R. da Silva, K. Bharuth-Ram, and L. M. C. Pereira, "Lattice location of implanted transition metals in 3C-SiC", J. Phys. D: Appl. Phys. **50**, 215101 (2017).

[23] A. R. G. Costa, U. Wahl, J. G. Correia, E. David-Bosne, L. M. Amorim, V. Augustyns, D. J. Silva, M. R. da Silva, and L. M. C. Pereira, "Lattice sites of ion-implanted Mn, Fe and Ni in 6H-SiC", Semic. Sci. Technol. **33**, 015021 (2018).

[24] M. Laube, F. Schmid, G. Pensl, G. Wagner, M. Linnarsson, and M. Maier, "Electrical activation of high concentrations of N^+ and P^+ ions implanted into 4H-SiC", J. Appl. Phys. **92**, 549-554 (2002).

[25] A. Debelle, L. Thomé, D. Dompoint, A. Boulle, F. Garrido, J. Jagielski, and D. Chaussende, "Characterization and modelling of the ion-irradiation induced disorder in 6H-SiC and 3C-SiC single crystals", J. Phys. D: Appl. Phys. **43**, 455408 (2010).

[26] J. Meier, D. Forkel-Wirth, T. Licht, U. Reislöhner, M. Uhrmacher, W. Witthuhn, ISOLDE Collaboration, "Perturbed-angular-correlation spectroscopy on indium and cadmium-complexes in silicon carbide", Mat. Res. Soc. Symp. Proc. **339**, 613–618 (1994).

[27] T. Licht, N. Achtziger, D. Forkel-Wirth, K. Freitag, J. Grillenberger, M. Kaltenhäuser, U. Reislöhner, M. Rüb, M. Uhrmacher, W. Witthuhn, and ISOLDE Collaboration, "Hafnium, cadmium and indium impurities in 4H-SiC observed by perturbed angular correlation spectroscopy", Diam. Rel. Mater. **6**, 1436-1439 (1997).

[28] N. Achtziger, D. Forkel-Wirth, J. Grillenberger, T. Licht, and W. Witthuhn, "Identification of deep band gap states in 4H- and 6H-SiC by radio-tracer DLTS and PAC-spectroscopy", Nucl. Instruments Methods Phys. Res. B **136–138**, 756–762 (1998).

[29] D. Åberg, A. Hållen, P. Pellegrino, and B. G. Svensson, "Nitrogen deactivation by implantation-induced defects in 4H-SiC epitaxial layers", Appl. Phys. Lett. **78**, 2908-2910 (2001).

[30] M. Ikeda, H. Matsunami, and T. Tanaka, "Site effect on the impurity levels in SiC", Phys. Rev. B **22**, 2842–2854 (1980).

[31] I. G. Ivanov, A. Henry, and E. Janzén, "Ionization energies of phosphorus and nitrogen donor and aluminium acceptors in 4H silicon carbide from the donor-acceptor pair emission", Phys. Rev. B **71**, 241201 (2005).

[32] G. L. Harris, Properties of Silicon Carbide (INSPEC, Exeter, 1995), chapter 7, pp. 155.

[33] G. Lindner, H. Hofsäss, S. Winter, B. Besold, E. Recknagel,G.Weyer, and J. W. Petersen, "Direct evidence for substitutional ion-implanted indium dopants in silicon", Phys. Rev. Lett. **57**, 2283–2286 (1986).

[34] E. Alves, M. F. da Silva, J. May, V. Haslar, P.Seidl, U. Feuser, and R. Vianden, "Epitaxial regrowth and lattice location of indium implanted in arsenic-preamorphized silicon", Nucl. Instruments Methods Phys. Res. B **55**, 580–584 (1991).

[35] H. Hofsäss, M. Restle, U. Wahl, and E. Recknagel, "Lattice location and annealing studies of heavy ion implanted diamond", Nucl. Instruments Methods Phys. Res. B **80–81**, 176–179 (1993).

[36] H. Quintel, K. Bharuth-Ram, H. Hofsäss, M. Restle, and C. Ronning, "Emission channeling study of annealing of radiation damage in heavy-ion implanted diamond", Nucl. Instruments Methods Phys. Res. B **118**, 72–75 (1996).

[37] K. Bharuth-Ram, A. Burchard, M. Deicher, H. Quintel, M. Restle, H. Hofsäss, and C. Ronning, "Implantation sites of In, Cd and Hf ions in diamond", Phys. Rev. B **64**, 195207 (2001).

[38] B. P. Doyle, E. J. Storbeck, U. Wahl, S. H. Connell, J. P. F. Sellschop, and the ISOLDE

collaboration, "Study of indium–defect interactions in diamond using two-dimensional conversion-electron emission channelling", J. Phys.: Condens. Matter **12** (2000) 67–78.

[39] R. Kalish, A. Reznik, S. Prawer, D. Saada, and J. Adler, "Ion-implantation-induced defects in diamond and their annealing: experiment and simulation", Phys. Stat. Sol. A **174**, 83–89 (1999).

[40] L. Pelaz, L. A. Marqués, and J. Barbolla, "Ion-beam-induced amorphization and recrystallization in silicon", J. Appl. Phys. **96**, 5947–5976 (2004).

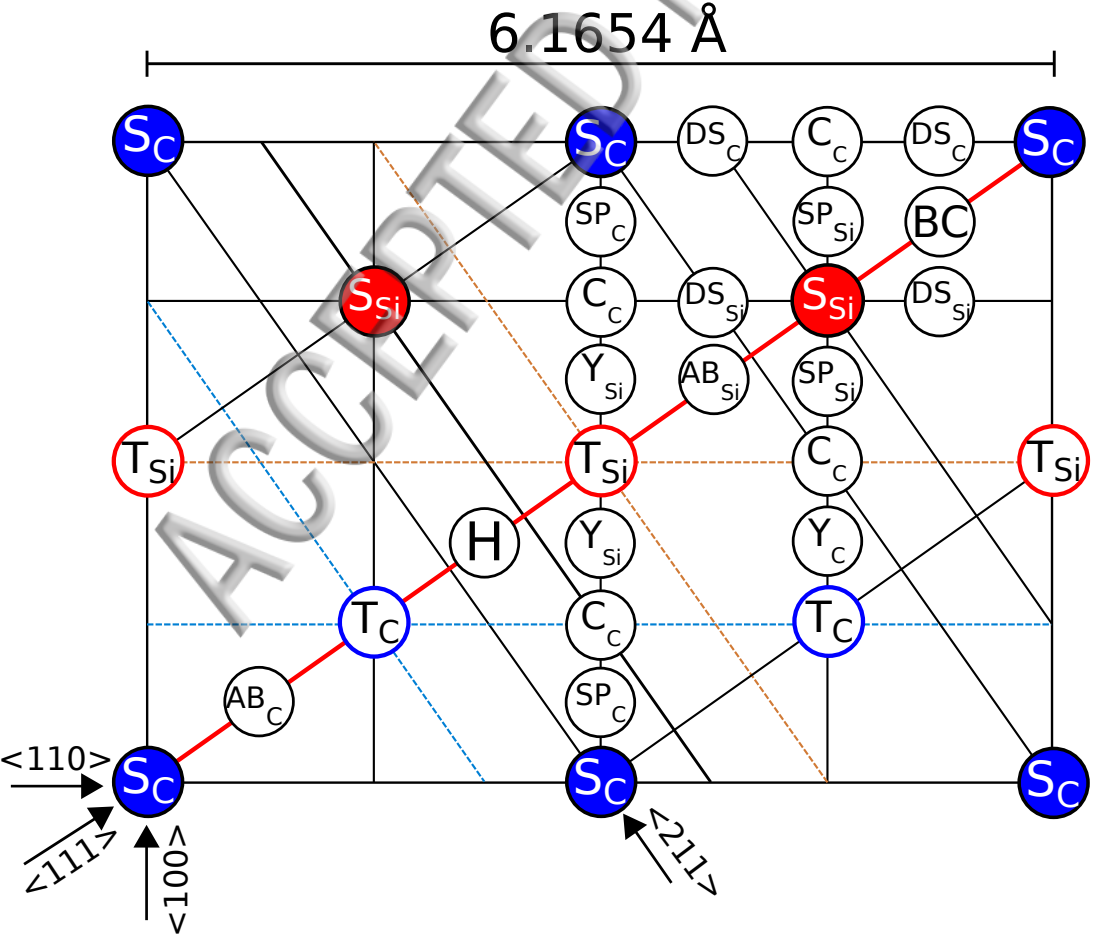

{110}plane in 3C-SiC zincblende lattice

S_{Si}, S_C: substitutional
AB_{Si}, AB_C: anti-bonding
BC: bond center
H: hexagonal
C_{Si}, C_C: "C"-site (C2v symmetry)
T_{Si}, T_C: tetrahedral interstitial
Y_{Si}, Y_C: "Y" or "Yb"-sites
DS_{Si}, DS_C <110>-displaced from S
SP_{Si}, SP_C: split <100>